



Graphene-Au-Coated Plasmonic Sensor Based on D-Shaped Bezier Polygonal Hollow Core Photonic Crystal Fiber

J. Divya¹ · S. Selvendran¹ · A. Sivanantha Raja² · A. Sivasubramanian¹

Received: 16 May 2021 / Accepted: 28 July 2021 / Published online: 4 August 2021
© Sociedade Brasileira de Física 2021

Abstract

A D-shaped photonic crystal fiber (PCF)-based plasmonic sensor is proposed for detecting refractive index (RI) variations within the range of 1.33–1.38. The center hollow core has formed using Bezier curves, which confines light within the core by the principle of photonic band gaps. An analyte is injected into a core to adjust its refractive index. Light propagating in the air core is affected by the analyte filled in the core, causing plasmon waves to be produced on the metal surface. On top of this structure, a chemically stable gold (Au) metal layer is placed as a plasmonic material. Numerical studies are carried out using the finite element method (FEM). The gold layer thickness is optimized and obtained an average sensitivity of 5600 nm/RIU. The sensor's sensitivity is enhanced by sandwiching graphene between an analyte and a gold film. The average sensitivity of the sensor increases by 2000 nm/RIU after graphene is incorporated, having reached 7600 nm/RIU according to the results obtained. The sensor can efficiently detect slight variations in the analyte indices and, thus, it is used in various chemical and biosensing applications.

Keywords Photonic crystal fiber · Surface plasmon resonance · Plasmonic sensor · Gold · Graphene

1 Introduction

Photonic crystal fiber (PCF)-based devices have been developed in recent years due to their flexibility and controllability. Unlike optical fiber, PCF has a flexible structure and a number of desirable properties, such as endless single mode, high nonlinearity, high birefringence, large mode field size, ease of filling material, low transmission loss, and controllable dispersion [1–3]. Hollow-core PCF (HCPCF) and non-hollow-core PCF (NHPCF) are the two most common types of PCF [4, 5]. In HCPCF, array of air holes in center act as a core and the silica material is filled in cladding regions with air holes. In NHPCF, instead of air holes, it has a silica core that is surrounded by air holes [6]. HCPCF use the photonic bandgap (scattering) method for signal propagation, whereas NCHCF uses the index guiding method (total internal reflection). In both

cases, the difference in refractive index causes the PCF to act as a waveguide, allowing a particular band of light to pass through it [7]. The bands of light propagated can be controlled by adjusting the size and position of the air holes [8].

PCFs are most often used in communications, but their uses have since grown to include sensors [9], polarization filters [10], multiplexer and demultiplexer [11], and other fields. A PCF can be used as a sensor by using the surface plasmon resonance (SPR) concept. Metals such as gold (Au), silver (Ag), copper (Cu), aluminum (Al), indium (In), and sodium (Na) are capable of producing surface plasmons (SPs) at the metal and dielectric boundary. These SPs have an oscillating nature and, under certain resonance conditions, have a tendency to propagate at metal surfaces [12]. Because of its higher sensitivity to the refractive index (RI) of the substrate in contact with plasmonic material, SPR techniques are commonly used in many sensing applications. The accuracy and resolution of sensor detection are affected by sensitivity, which is one of the most critical performance parameters of sensors. The PCF-surface plasmon resonance (SPR) sensor's sensitivity can be increased by coating plasmonic material on the inner wall of air holes, which is a difficult task. To

✉ J. Divya
divyaselva0605@gmail.com

¹ SENSE, Vellore Institute of Technology, Chennai,
Tamil Nadu 600127, India

² Alagappa Chettiar Government College of Engineering
and Technology, Tamil Nadu, Karaikudi 630 003, India

address these problems, D-shaped PCF sensors have been proposed; the top circular portion of the fiber with air holes has been fully removed and then polished. The polished surface is coated with plasmonic material and a sensing layer. Air holes are placed at regular intervals to guide the light propagation in a specific direction [13]. A dual-core D-shaped PCF sensor was proposed by Md. Nazmus et al. The gold thickness was optimized, and a wavelength sensitivity of 8000 nm/RIU was obtained [14]. Emranul Haque, et.al., designed a SPR-based PCF sensor. A gold (Au) layer was coated in an open ring placed in top of the D-shaped PCF structure for simple detection. RIs of analyte ranging from 1.18 to 1.36 and 20,000 nm/RIU wavelength sensitivity and 1054 RIU⁻¹ maximum amplitude sensitivity were obtained [15].

Rather than increasing the thickness of the metal film, nanomaterials, such as graphene, are incorporated with the metal surface and decrease the cost or narrow down the spectrum. When in contact with an analyte, efficient charge transfer can cause strong coupling and increased sensitivity at the metal-graphene interface, which can lead to an increase in SPR [16]. As a result, a variety of PCF structures have been proposed. For example, Bin Li et al. proposed an SPR-based liquid refractive index sensor by depositing a controllable thickness gold film and then coating it with graphene. After the addition of graphene, the sensor's sensitivity increases by 390 nm/RIU, resulting in a final sensitivity of 2290 nm/RIU [17]. A graphene-Au-coated

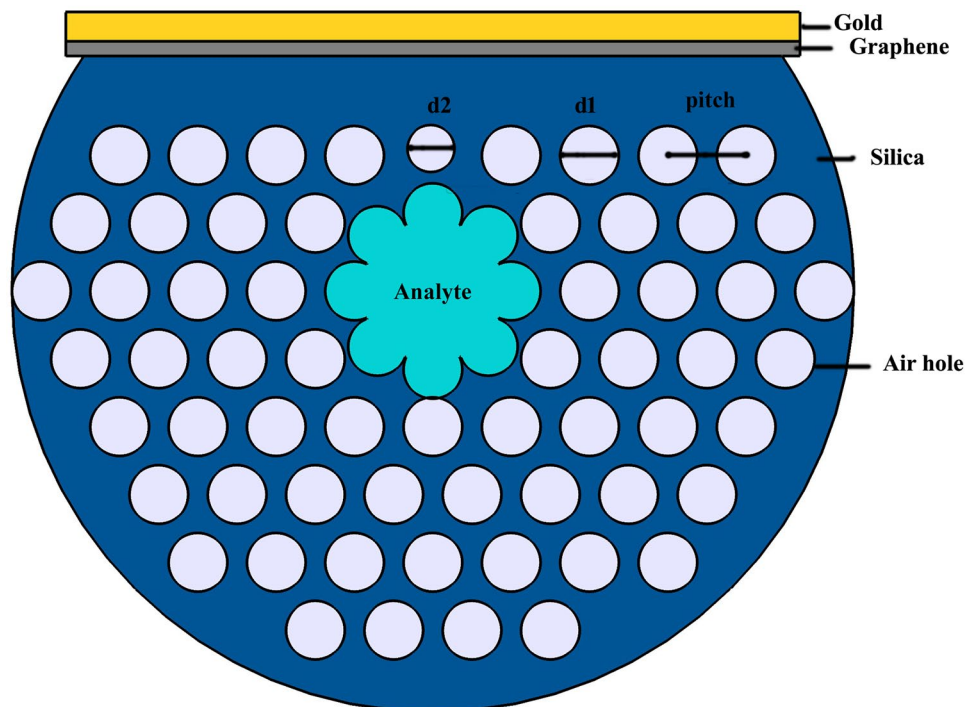
photonic crystal fiber (PCF) sensor had been developed by Hongyan Yang et al. Meanwhile, graphene on gold can stably adsorb biomolecules and increase SPR; it can improve sensor sensitivity achieving wavelength sensitivity of 4200 nm/RIU and amplitude sensitivity of 450 RIU⁻¹ [18].

We propose a plasmonic sensor based on a D-shaped HCPCF with a center core built using Bezier curves that can detect small RI variations in analyte over a range of 1.33–1.38 in this paper. This sensor is used for biosensing applications due to its wide range of RI variations. The finite element (FEM) approach is used to conduct numerical investigations. Simultaneously, various optimization strategies, such as gold and graphene layer thickness, are calculated. An optimal plasmonic sensor structure is obtained. Coating graphene between an analyte and the gold film improves the sensor's sensitivity. The average sensitivity of the sensor increased by 2000 nm/RIU and reached 7600 nm/RIU. Following the introduction chapter, Sect. 2 summarizes the D-shaped fiber design. The results of various optimization techniques are discussing in Sect. 3. Finally, in Sect. 4, we conclude the outcome and possible progress based on the results.

2 Modeling of D-Shaped HCPCF Sensor

Figure 1 shows a schematic diagram of the proposed D-shaped HCPCF sensor. A hexagonal structure with 0.6- μm diameter air holes (d_1) arranged in a triangular

Fig. 1 Schematic diagram of the proposed D-shaped hollow core photonic crystal fiber sensor



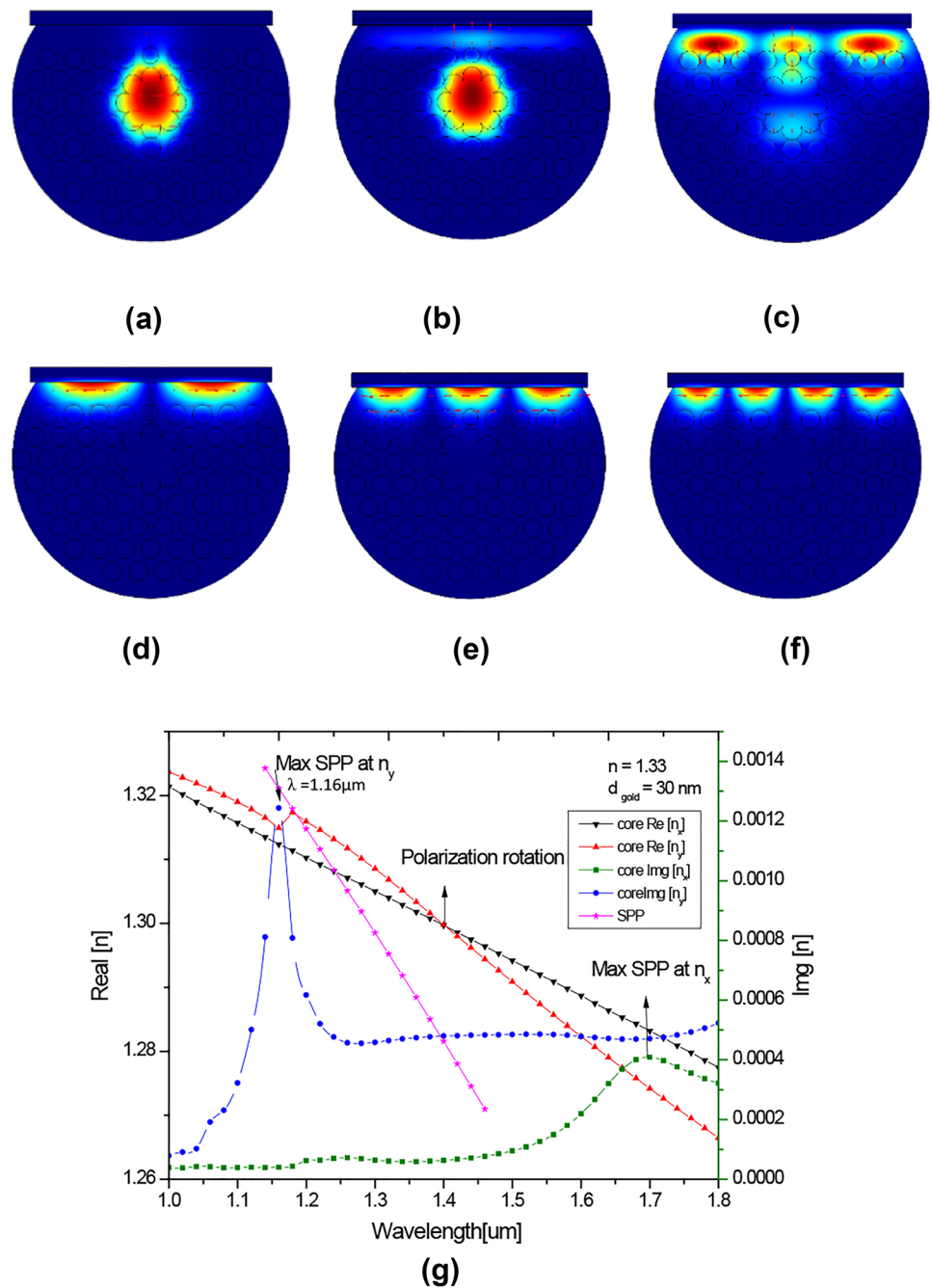
lattice, and the lattice constant (Λ) (distance between the centers of successive air holes) of $0.8 \mu\text{m}$. Instead of traditional circles, the middle hollow core is a complicated Bezier polygon structure. Bezier polygon structures are derived using a circular lattice structure with air holes of $0.6\text{-}\mu\text{m}$ diameter, and the lattice constant (Λ) of $0.8 \mu\text{m}$ by keeping an angle of separation of 45° each between them.

The fiber's core is a Bezier polygon structure that works in Dirac mode, a new light trapping technique. The Dirac mode's unique power-law profile allows for

loose lateral containment, allowing for long-range interaction between multiple cores. This property leads to the novel coupling and sensing properties for use in optical couplers, laser arrays, and fiber sensors [19]. By filling the air core with the analyte, the hollow core fiber can be used as a sensor.

To construct a D-shape, the top circular portion of the fiber with air holes has been fully removed. Gold is used as a plasmonic material because it is chemically stable. The gold layer that has a thickness of 30 nm is placed on the top of the structure. Because of its high surface-to-volume

Fig. 2 The simulated (a) x-polarized core mode, (b) y-polarized core mode, (c) coupling mode, (d) 1-SPP mode, (e) 2-SPP mode, (f) 3-SPP mode, and (g) real and imaginary parts of n_{eff} as a function of wavelength for analyte RI of 1.33



ratio, broadband optical, and plasmonic properties [20], graphene is coated between the analyte and the gold layer to improve sensing efficiency. Graphene has a thickness of 15 nm. The indices of the analyte put in the core affect light propagation through the air core. The formation of surface plasmon polaritons (SPP) causes light coupled from the core mode to the gold surface. At this phase matching point, the wave vectors of both the light wave and the plasmon wave are the same, so the optimum coupling is observed. The sensor’s smaller central air hole of 0.4- μm diameter (d_2) is allows the passing wave to penetrate and enter the metal–dielectric interface, which can excite more free electrons. Scattering boundary conditions are established to minimize scattering losses to achieve higher accuracy. The COMSOL Multiphysics software, which is based on the finite element method (FEM), is used for simulation and performance analysis. The proposed D-shaped PCF sensor can be directly fabricated either by halfway stacking [21] or by fabricated a regular PCF followed by mechanical side polishing methods [22]. The desired gold layer and graphene layer can be deposited using the chemical vapor deposition method [23]. The analyte can be filled in the center air hole by vacuum pumping technique [24] or infiltration method [25].

The refractive index values for base silica and gold are obtained using the Sellmeier equation [26] and Lorentz–Drude model [27]. The complex refractive index equation of graphene is [28]

$$n_g = \frac{3 + iC_1\lambda}{3}$$

where n_g denotes the RI of graphene, λ (μm) is the wavelength, and $C_1 \approx 5.446 \mu\text{m}^{-1}$.

3 Results and Discussion

3.1 Mode Coupling

A change in the RI of the analyte causes a shift in the phase matching point of plasmon mode and core mode. As a

consequence, the resonance wavelength varies depending on the analyte RI, determining the PCF’s sensing operation [29]. The electric field distributions of x-polarized core mode and y-polarized core mode, respectively, are shown in Fig. 2a, b, where the light is restricted to the core region. In y-polarization, the coupling efficiency between the SPP mode and the core mode is higher than in x-polarization. Therefore, we consider a y-polarized core mode for study. Figure 2c depicts the coupled modes. At the moment, the core mode is phase-matched with the plasmon mode, a resonance peak will appear, and the energy in the core mode will be transferred to the plasmon mode. There exists a first-order SPP mode, a second-order SPP mode, and a third-order SPP mode in the PCF sensor that are as shown in Fig. 2d-f.

Figure 2g represents the dispersion relation between the fundamental mode and SPP mode. The real and imaginary values of the effective mode index (n_{eff}) and as a function of wavelength for analyte RI of 1.33 are represented. We found that as the wavelength increases, the real part of the n_{eff} of the core guided mode decreases. At a wavelength of 1160 nm, a slight tilt (S curve) in the real value of n_{eff} indicates that the fiber’s core mode is in resonance with the plasmon mode. As a result, a portion of the light is coupled into the SPP mode, resulting from loss in fundamental mode. At this point, the imaginary value of n_{eff} reaches its maximum value, which is the resonance wavelength (1160 nm).

Confinement loss [30] is an important parameter to consider when evaluating the sensor’s performance, and is defined as

$$\text{Confinement Loss} = \frac{40 \times \Pi \times \text{Im}(n_{\text{eff}}) \times 10^4}{\lambda \times \ln(10)} \text{ (dB/cm)}$$

where $\text{Im}(n_{\text{eff}})$ is the imaginary part of effective mode index.

3.2 Numerical Examination on the Varying Thicknesses of the Gold Layer

The thickness of metal has a significant effect on the efficiency of plasmonic sensors. The gold film thickness affects the sensor’s confinement loss and resonance wavelength. Table 1 shows the analysis of the different thicknesses of

Table 1 Analysis of the sensor for the different thicknesses of gold layer for refractive index 1.33 and 1.34

Gold layer thickness (nm)	Refractive index (n) = 1.33		Refractive index (n) = 1.34		Sensitivity (nm/RIU)
	Resonance wavelength (nm)	Confinement loss (dB/cm)	Resonance wavelength (nm)	Confinement loss (dB/cm)	
10	1120	590.25	1100	522.47	2000
20	1140	625.05	1120	556.55	2000
30	1160	675.35	1100	602.33	6000
40	1180	633.76	1140	486.88	4000
50	1180	547.95	1140	416.28	4000

Fig. 3 (a) Loss spectrum curve of gold layer thickness (20 nm, 30 nm, and 40 nm) which changes with wavelength. (b) Confinement loss factors with respect to wavelength for different RI of analyte ranging from 1.33 to 1.38

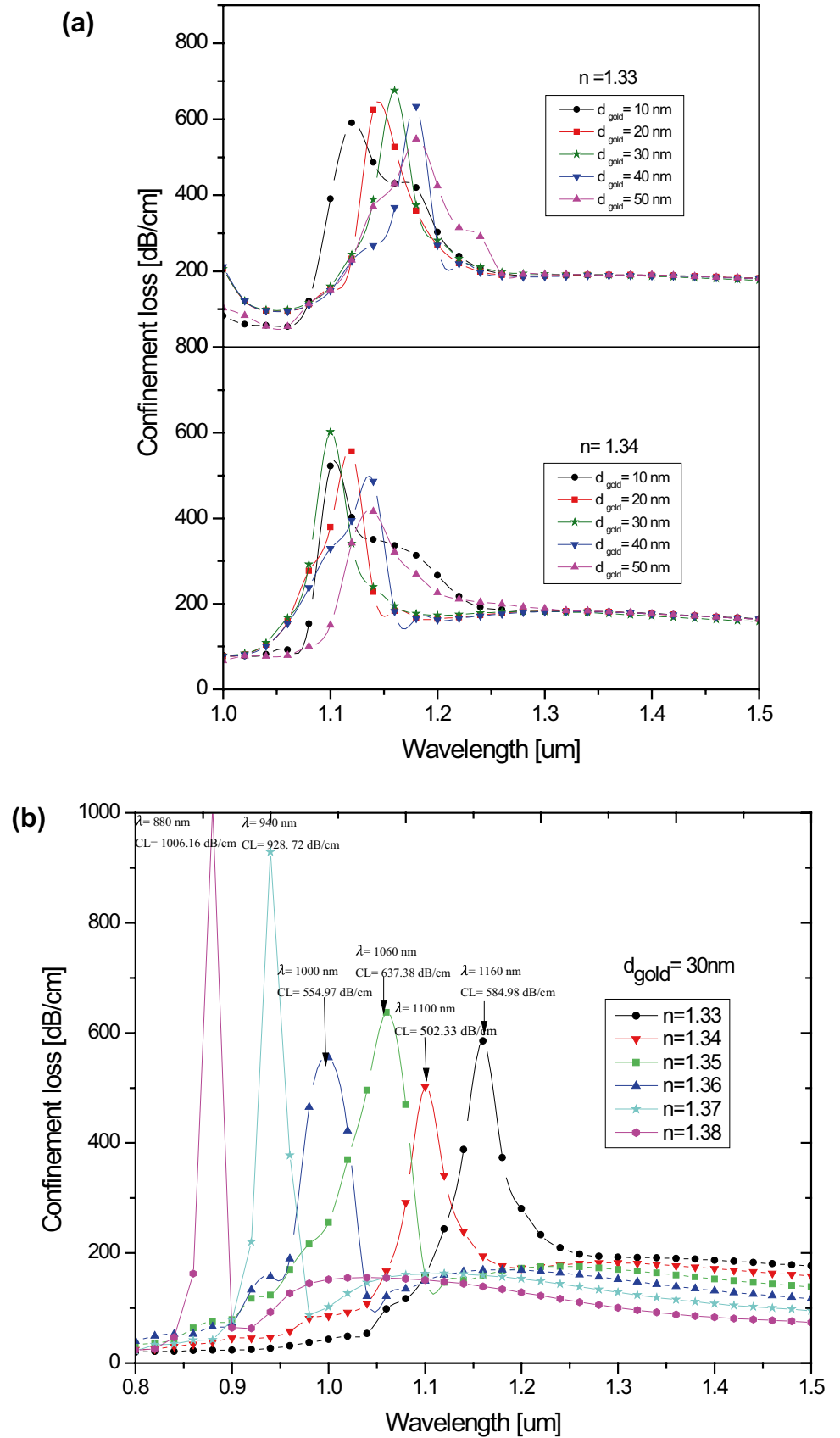
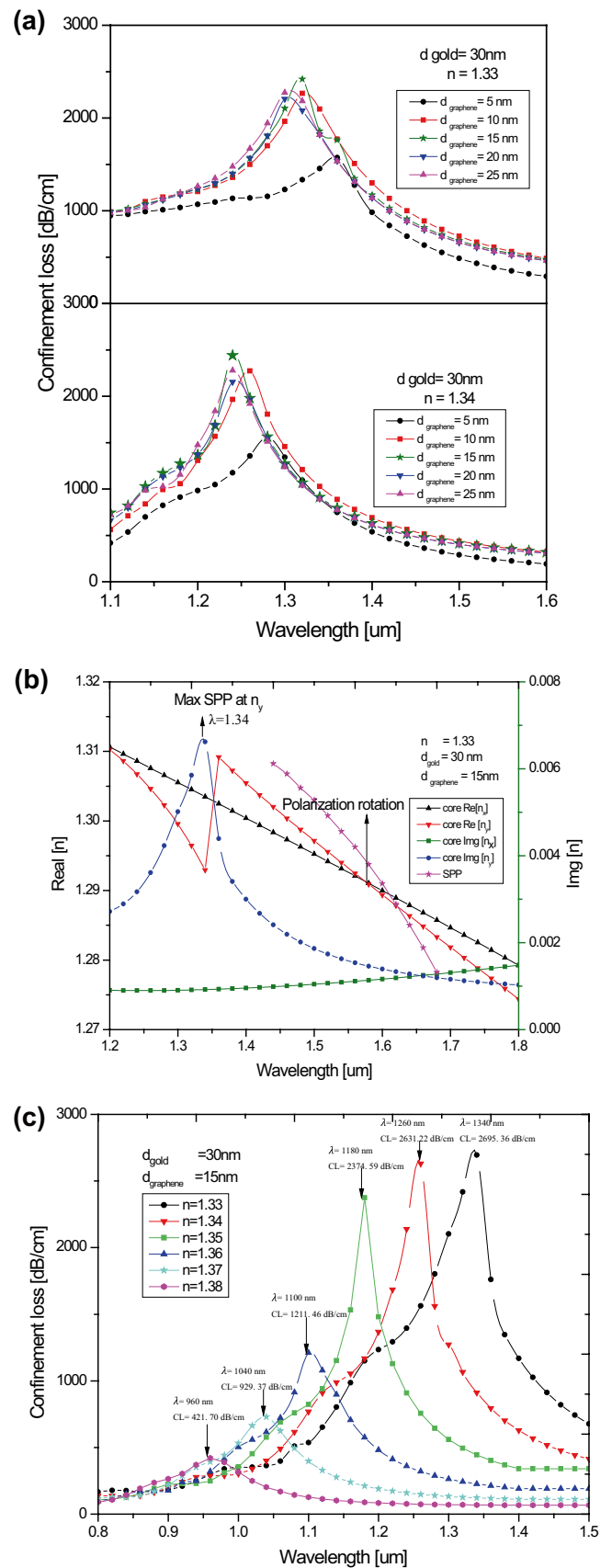


Fig. 4 (a) Loss spectrum curve of Graphene thickness (5 nm, 10 nm, and 15 nm) which changes with wavelength. (b) Real and imaginary parts of n_{eff} as a function of wavelength for analyte RI of 1.33 (gold layer along with graphene ($d_{\text{gold}}=30$ nm and $d_{\text{graphene}}=15$ nm)). (c) Confinement loss factors with respect to wavelength for different RI of analyte ranging from 1.33 to 1.38



the gold layer. Figure 3a depicts the comparison of the different thicknesses (10, 20, 30, 40, and 50 nm) of gold films. It shows that the confinement loss of PCF decreases as the gold film thickness increases.

The sensitivity of sensor [31] can be calculated by

$$S_\lambda = \frac{\Delta\lambda_{\text{peak}}}{\Delta n_a} \text{ (nm/RIU)}.$$

$\Delta\lambda_{\text{peak}}$ is the shift in resonance wavelength and Δn_a is the shift in analyte RI value.

From Table 1, the maximum sensitivity of 6000 nm/RIU is observed for 30-nm gold layer thickness. So, $d_{\text{gold}} = 30$ nm is used for further analysis to improve sensing performance.

Figure 3b represents the loss spectrum of the proposed sensor coated with gold for different analyte RIs ranging from 1.33 to 1.38 with a step value of 0.01. As the RI increases, the resonance wavelength shifts towards shorter wavelengths. For the analyte RI value of about 1.34, the observed minimum confinement loss is 502.33 dB/cm at a resonance wavelength of 1100 nm. And the maximum confinement loss of 1006.16 dB/cm has been noticed at a peak resonance wavelength of 880 nm for an RI value of 1.38. These results describe that for the analyte RI value of 1.38, the phase-matching condition has been realized between the core mode to SPP mode at resonance wavelength 880 nm. And the maximum energy transfer takes place between core and SPP mode.

3.3 Numerical Examination on the Varying Thickness of Graphene Layer

As mentioned previously, graphene is layered on the gold film; efficient charge transfer can take place in the gold-graphene interface. The resonance wavelength can be modified by increasing SPR. And the sensor’s sensitivity has increased. The thickness of the graphene with gold film ($d_{\text{gold}} = 30$ nm) affects the sensor’s confinement loss and resonance wavelength. Table 2 represents the analysis of the different thickness of graphene layer along with the gold layer ($d_{\text{gold}} = 30$ nm). Figure 4a shows the comparison of the

thickness of 5, 10, 15, 20, and 25 nm graphene. It shows that as the graphene thickness increases, the sensor’s confinement loss also increases.

From Table 2, the maximum sensitivity of 8000 nm/RIU is observed for graphene thickness of 5 and 15 nm, but the peak gets broaden in 5-nm thickness. Broadening of loss peak may reduce the detection accuracy. Therefore, $d_{\text{graphene}} = 15$ nm is using for better sensing performance.

Figure 4b shows the dispersion relation between the fundamental mode and SPP mode. The real and imaginary values of the effective mode index (n_{eff}) and as a function of wavelength for analyte RI of 1.33 are represented. We observed that as the wavelength increases, the real part of the n_{eff} of the core guided mode decreases. At a wavelength of 1340 nm, a deep tilt (S curve) in the real value of n_{eff} indicates that the fiber’s core mode is in resonance with the plasmon mode. As a result, a portion of the light is coupled into the SPP mode, resulting from loss in fundamental mode. At this point, the imaginary value of n_{eff} reaches its maximum value, which is the resonance wavelength (1340 nm).

Figure 4c represents the loss spectrum of the proposed sensor coated with gold and graphene for different analyte RIs ranging from 1.33 to 1.38 with a step value of 0.01. As the RI increases, the resonance wavelength shifts towards shorter wavelengths. For the analyte RI value of about 1.38, the observed minimum confinement loss is 421.70 dB/cm at a resonance wavelength of 960 nm. And the maximum confinement loss of 2695.36 dB/cm has been noticed at a peak resonance wavelength of 1340 nm for an RI value of 1.33. These results describe that for the analyte RI value of 1.33, the phase-matching condition has been realized between the core mode to SPP mode at resonance wavelength 1340 nm. And the maximum energy transfer takes place between core and SPP mode.

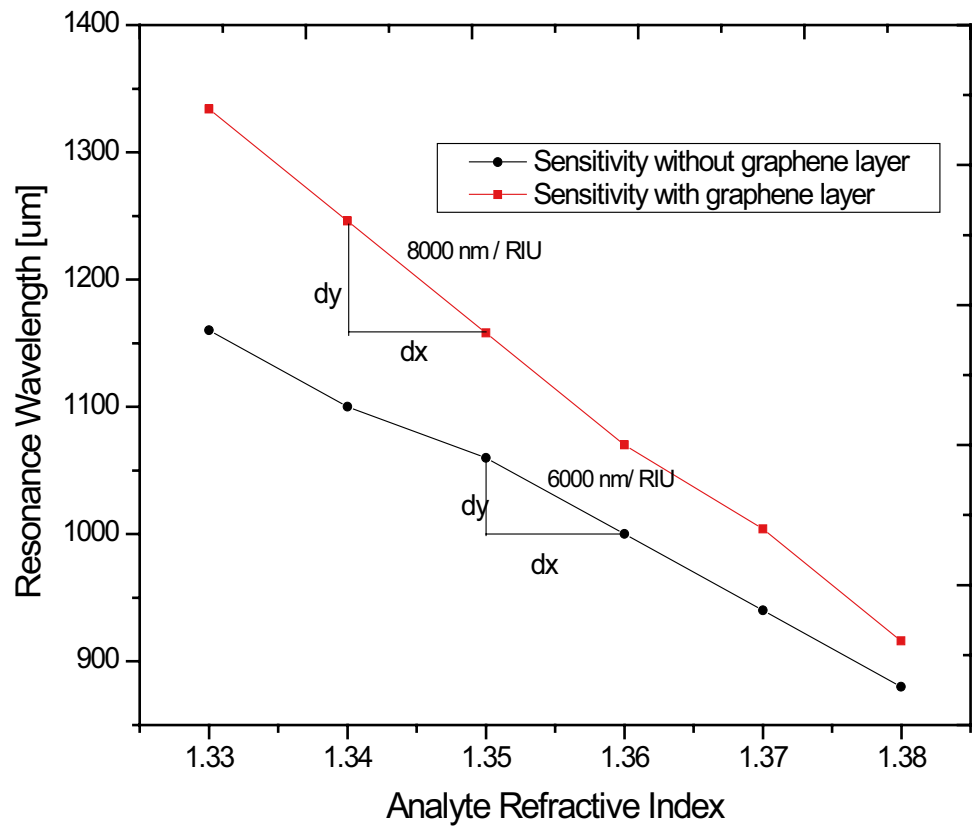
3.4 Comparative Analysis of With and Without Graphene Layer

The sensor structure was compared with and without graphene coating using the same structural parameters. Figures 2g and 4b show the real and imaginary values of

Table 2 Analysis of the sensor for the different thicknesses of graphene layer along with gold layer thickness of 30 nm for refractive index 1.33 and 1.34

Graphene layer thickness (nm)	Refractive index (n)= 1.33		Refractive index (n)= 1.34		Sensitivity (nm/RIU)
	Resonance wavelength (nm)	Confinement loss (dB/cm)	Resonance wavelength (nm)	Confinement loss (dB/cm)	
5	1360	1571.86	1280	1558.02	8000
10	1320	2264.90	1260	2471.98	6000
15	1340	2695.36	1260	2631.22	8000
20	1300	2206.78	1240	2154.61	6000
25	1300	2271.87	1240	2277.60	6000

Fig. 5 Resonance wavelength vs analyte RI for sensor sensitivity measurement



effective mode index (n_{eff}) as a function of wavelength for analyte RI of 1.33 when the sensor is coated with gold ($d_{gold} = 30$ nm) and gold along with graphene ($d_{gold} = 30$ nm and $d_{graphene} = 15$ nm). A tilt (S curve) in the real value of n_{eff} shows that the core mode of the fiber is in resonance with the plasmon mode. A portion of the light is coupled into the SPP mode, and hence, there is a loss in fundamental mode. In Fig. 4b, the real value of n_{eff} has a long drift than a n_{eff} value in Fig. 2g, which shows that gold along with graphene has a high resonance wavelength of SPR than the gold alone structure; this leads to enhanced sensitivity.

For further analysis, Figs. 3b and 4c represent the loss spectrum for different analyte RIs ranging from 1.33 to 1.38

with a step value of 0.01 for both structures (with and without graphene). It shows when the sensor has coated with a gold layer, the resonance wavelength ranging from 880 to 1160 nm. Its maximum sensitivity is 6000 nm/RIU, and its average sensitivity is about 5600 nm/RIU. After graphene has layered, the resonance wavelength ranging from 960 to 1340 nm. The maximum sensitivity is 8000 nm/RIU, and its average sensitivity is about 7600 nm/RIU. Compared to the results of sensitivity, the presence of graphene enhances the sensitivity and improves the performance of detection.

Figure 5 illustrates the variation in sensitivity for the different wavelengths. It shows that sensitivity reaches the maximum value of 8000 nm/RIU for the gold layer thickness

Table 3 Performance comparison with previously reported D-shaped plasmonic sensors

Authors	Year	Structure used	Material used	RI detection range (n)	Sensitivity (nm/RIU)
Hongyen Yang et al. [18]	2021	D-shaped PCF sensor	Gold-graphene	1.32–1.41	4200
Xiangtai Xi et al. [29]	2020	D-shaped SPR biosensor	Gold-graphene	1.33–1.36	1223
Bin Li et al. [17]	2019	D-shaped RI sensor	Gold-graphene	1.33–1.36	2290
Singh et al. [27]	2019	D-shaped sensor	Gold-graphene	1.32–1.35	5666
Junxia Sun et al. [30]	2019	D-shaped SPR sensor	Gold-graphene	1.33–1.36	1539
Guowen An et al [28]	2018	D-shaped RI sensor	Gold-graphene	1.33–1.39	4391
Our proposed work		D-shaped Hollow core PCF sensor	Gold-graphene	1.33–1.38	For Gold: 5600 For gold and graphene: 7600

of 30 nm coated with a graphene layer thickness of 15 nm. It is due to the enhancement of the confined electric field onto the top surface of the sensor.

Performance comparison with previously reported D-shaped plasmonic sensors is detailed in Table 3. Our proposed sensor structure yields a sensitivity value of 7600 nm/RIU, which is much better than the previously reported sensors [17, 18, 28, 32–34].

4 Conclusion

In conclusion, we proposed a D-shaped hollow-core PCF-based plasmonic sensor, with the analyte filled in the central core. By changing the analyte's RI, the resonance wavelength has changed. SPR is initially generated by the gold film, but with an optimized gold layer thickness, sensitivity has improved. In the refractive index range of 1.33 to 1.38, an average sensitivity of 5600 nm/RIU has obtained. After that, we coated a graphene layer between the analyte and the gold film. The sensor's average wavelength sensitivity increased by 2000 nm/RIU and reaching 7600 nm/RIU. It is proven that graphene can be used to not only prevent gold from oxidation but also, to improve sensing efficiency. Since the sensor can detect minor changes in analyte indices, it can be used in various chemical and biosensing applications.

References

1. J. Yang, L. Zhou, X. Che, J. Huang, X. Li, W. Chen, Photonic crystal fiber methane sensor based on modal interference with an ultraviolet curable fluoro-siloxane nano-film incorporating cryptophane A. *Sens. Actuators B Chem.* **235**, 717–722 (2016). <https://doi.org/10.1016/j.snb.2016.05.125>
2. T. Cheng, Z. Duan, M. Liao, W. Gao, D. Deng, T. Suzuki, Y. Ohishi, A simple all-solid tellurite microstructure optical fiber. *Opt. Express* **21**, 3318–3323 (2013). <https://doi.org/10.1364/OE.21.003318>
3. W.C. Wong, C.C. Chan, L.H. Chen, T. Li, K.X. Lee, K.C. Leong, Polyvinyl alcohol coated photonic crystal optical fiber sensor for humidity measurement. *Sens. Actuators B Chem.* **174**, 563–569 (2012). <https://doi.org/10.1016/j.snb.2012.07.032>
4. H. Chen et al., A novel polarization splitter based on dual-core photonic crystal fiber with a liquid crystal modulation core. *IEEE Photon J.* **6**(4), 2201109 (2014). <https://doi.org/10.1109/JPHOT.2014.2337874>
5. B. Eggleton, C. Kerbage, P. Westbrook, R. Windeler, A. Hale, Microstructure optical fiber devices. *Opt. Express* **9**, 698–713 (2001). <https://doi.org/10.1364/OE.9.000698>
6. X. Zhang, R. Wang, F. Cox, B. Kuhlmeier, M. Large, Selective coating of holes in microstructure optical fiber and its application to in-fiber absorptive polarizers. *Opt. Express* **15**, 16270–16278 (2007). <https://doi.org/10.1364/OE.15.016270>
7. A. Hassani, M. Skorobogatiy, Design of the microstructure optical fiber-based surface plasmon resonance sensors with enhanced microfluidics. *Opt. Express* **14**, 11616–11621 (2006). <https://doi.org/10.1364/OE.14.011616>
8. H.W. Lee, M.A. Schmidt, R.F. Russell, N.Y. Joly, H.K. Tyagi, P. Uebel, P.S.J. Russell, Pressure assisted melt-filling and optical characterization of Au nano-wires in microstructure fibers. *Opt. Express* **19**, 12180–12189 (2011). <https://doi.org/10.1364/OE.19.012180>
9. S. Selvendran, A. Sivanantharaja, S. Yogalakshmi, A highly sensitive Bezier polygonal hollow core photonic crystal fiber biosensor based on surface plasmon resonance. *Optik – Int. J. Light and Electron Opt* **171**, 109–113 (2018). <https://doi.org/10.1016/j.ijleo.2018.06.039>
10. S. Yogalakshmi, S. Selvendran and A Sivanantha Raja, Design and analysis of a photonic crystal fiber-based polarization filter using surface plasmon resonance. *Laser Phys.* **26**(2016)
11. X. Qiang, K. Li, N. Copner, S. Lin, An ultrashort wavelength multi/demultiplexer via rectangular liquid-infiltrated dual-core polymer optical fiber. *Materials* **12**, 1709 (2019). <https://doi.org/10.3390/ma12101709>
12. U. Fano, The theory of anomalous diffraction gratings and of quasi-stationary waves on metallic surfaces. *J. Opt. Soc.* **31** (3) 213–222. <https://doi.org/10.1364/JOSA.31.000213>
13. M. Chen, T. Lang, B. Cao, Y. Yu, C. Shen, D-type optical fiber immunoglobulin g sensor based on surface plasmon resonance. *Opt. Laser Technol.* **131**, 106445 (2020). <https://doi.org/10.1016/j.optlastec.2020.106445>
14. M.N. Sakib, M.B. Hossain, K.F. Al-tabatabaie, I.M. Mehedi, M.T. Hasan, M.A. Hossain, I.S. Amiri, High performance dual core D-shape PCF-SPR sensor modeling employing gold coat. *Res. Phys.* **S2211–3797**(19)32981-X, <https://doi.org/10.1016/j.rinp.2019.102788>
15. E. Haque, M.A. Hossain, F. Ahmed, Y. Namihira, Surface plasmon resonance sensor based on modified d-shaped photonic crystal fiber for wider range of refractive index detection. *IEEE Sensors J.* <https://doi.org/10.1109/JSEN.2018.2865514>
16. B. Song, D. Li, W. Qi, M. Elstner, C. Fan, H. Fang, Graphene on Au (111): A highly conductive material with excellent adsorption properties for high-resolution bio/nano detection and identification. *Chem. Phys. Chem* **11**, 585–589 (2010). <https://doi.org/10.1002/cphc.200900743>
17. B. Li, T. Cheng, J. Chen, X. Yan, Graphene-enhanced surface plasmon resonance liquid refractive index sensor based on photonic crystal fiber. *Sensors* **19**, 3666 (2019). <https://doi.org/10.3390/s19173666>
18. H. Yang, M. Liu, Y. Chen, L. Guo, G. Xiao, H. Liu, J. Li, L. Yuan, Highly sensitive graphene-Au coated plasmon resonance PCF sensor. *Sensors* **21**, 818 (2021). <https://doi.org/10.3390/s21030818>
19. K. Xie, W. Zhang, A.D. Boardman, H. Jiang, Z. Hu, Y. Liu, M. Xie, Q. Mao, L. Hu, Q. Li, T. Yang, F. Wen, E. Wang, Fiber guiding at the Dirac frequency beyond photonic bandgaps. *Light: Sci. Appl.* **4** (2015) e304, <https://doi.org/10.1038/lsa.2015.77>
20. A.B. Kuzmenko, E. van Heumen, F. Carbone, D. van der Marel, Universal optical conductance of graphite. *Phys. Rev. Lett.* **100**, 117401 (2008). <https://doi.org/10.1103/PhysRevLett.100.117401>
21. N. Zhang, K. Li, Y. Cui, Z. Wu, P.P. Shum, J.L. Auguste, X.Q. Dinh, G. Humbert, L. Wei, Ultra-sensitive chemical and biological analysis via specialty fibers with built-in micro structured optofluidic channels. *Lab. Chip* **18**(4), 655–661 (2018). <https://doi.org/10.1039/C7LC01247K>
22. T. Huang, Highly sensitive SPR sensor based on D-shaped photonic crystal fiber coated with indium tin oxide at near-infrared wavelength. *Plasmonics* **12**(3), 583–588 (2017). <https://doi.org/10.1007/s11468-016-0301-7>

23. J. Boehm, A. François, H. Ebendorff-Heidepriem, T.M. Monro, Chemical deposition of silver for the fabrication of surface plasmon micro structured optical fibre sensors. *Plasmonics* **6**(1), 133–136 (2011). <https://doi.org/10.1007/s11468-010-9178-z>
24. New design for all-normal near zero dispersion photonic crystal fiber with selective liquid infiltration for broadband supercontinuum generation at 1.55 μm , Hindawi Publishing Corporation *Journal of Photonics*, Vol. 2014, Article ID 728592, <https://doi.org/10.1155/2014/728592>
25. T. Han, Y. Liu, Z. Wang, J. Guo, Z. Wu, S. Wang, Z. Li, W. Zhou, Unique characteristics of a selective-filling photonic crystal fiber Sagnac interferometer and its application as high sensitivity sensor. *Opt. Express* **21**(1), (2013) <https://doi.org/10.1364/OE.21.000122>
26. W. Sellmeier, To explain the abnormal color sequence in the spectrum of some substances. *Ann. Der. Phys.* **219**, 272–282 (1870)
27. F. Hao, P. Nordlander, Efficient dielectric function for FDTD simulation of the optical properties of silver and gold nanoparticles. *Chem. Phys. Lett.* **446**, 115–118 (2007)
28. S. Singh, Y.K. Prajapati, Highly sensitive refractive index sensor based on D-shaped PCF with gold-graphene layers on the polished surface. *Appl. Phys. A* **125**, 437 (2019). <https://doi.org/10.1007/s00339-019-2731-5>
29. S. Selvendran, A. Sivanantha Raja, S. Yogalakshmi, A highly sensitive surface plasmon resonance biosensor using photonic crystal fiber filled with gold nanowire encircled by silicon lining. *Optik* S0030–4026(17)31370–0. <https://doi.org/10.1016/j.ijleo.2017.10.157>
30. N. Chen, M. Chang, X.D. Zhang, J. Zhou, X.L. Lu, S.L. Zhuang, Highly sensitive plasmonic sensor based on a dual-side polished photonic crystal fiber for component content sensing applications. *Nanomaterials* **9**, 1587 (2019). <https://doi.org/10.3390/nano9111587>
31. C. Liu, W. Su, Q. Liu, X. Lu, F. Wang, T. Sun, P.K. Chu, Symmetrical dual D-shape photonic crystal fibers for surface plasmon resonance sensing. *Opt. Express* **26**, 9039–9049 (2018). <https://doi.org/10.1364/OE.26.009039>
32. G. An, S. Li, T. Cheng, X. Yan, X. Zhang, X. Zhou, Z. Yuan, Ultra-stable D-shaped optical fiber refractive index sensor with graphene-gold deposited platform. *Plasmonics* (2018). <https://doi.org/10.1007/s11468-018-0788-1>
33. X. Xi, Xu. Jihua, S. Li, J. Song, W. Yang, Y. Sun, S. Jiang, Y. Han, X. Fan, An Au nanofilm-graphene/D-type fiber surface plasmon resonance sensor for highly sensitive specificity bioanalysis. *Sensors* **20**, 991 (2020). <https://doi.org/10.3390/s20040991>
34. J. Sun, S. Jiang, Xu. Jihua, Z. Li, Yu. Chonghui Li, X.Z. Jing, J. Pan, C. Zhang, B. Man, Sensitive and selective SPR sensor employing gold-supported graphene composite film/D shaped fiber for dopamine detection. *J. Phys. D: Appl. Phys* (2019). <https://doi.org/10.1088/1361-6463/ab08c1>

Publisher's Note Springer Nature remains neutral with regard to jurisdictional claims in published maps and institutional affiliations.